

Influence of SnO₂ nanoparticles incorporation on the Electrochemical Behaviour of a Superconductor in Sodium Sulphate Solutions

H. T. Rahal¹, A. M. Abdel-Gaber^{1,2,*}, R. Awad³

¹ Department of Chemistry, Faculty of Science, Beirut Arab University, P.O. Box 11-5020 Riad El Solh 11072809 - Beirut, Lebanon

² Department of Chemistry, Faculty of Science, Alexandria University, Ibrahimia, P.O. Box 426, Alexandria 21321, EGYPT

³ Department of Physics, Faculty of Science, Beirut Arab University, P.O. Box 11-5020 Riad El Solh 11072809 - Beirut, Lebanon

*E-mail: ashrafmoustafa@yahoo.com; a.abdelgaber@bau.edu.lb

Received: 11 July 2017 / Accepted: 9 September 2017 / Published: 12 October 2017

The influence of SnO₂ nanoparticles addition on the corrosion and capacitive behaviour of (SnO₂)_x(Bi,Pb)-2223, where x=0.00, 0.025, and 0.1wt. % phase superconductor in 0.1 mol L⁻¹ Na₂SO₄ at 30⁰C was studied using potentiodynamic polarization curves measurements, cyclic voltammetry and electrochemical impedance spectroscopy (EIS) techniques. . The prepared samples were characterized by X-ray diffraction (XRD), transmission electron microscopy (TEM) as well as scanning electron microscopy (SEM). XRD patterns showed that nano-sized SnO₂ are located at the surface and grains boundaries reducing the voids present in the (Bi,Pb)-2223 matrix as displayed by SEM photographs. Such fact is confirmed by TEM images that also assured the presence of nanosized SnO₂ particles in the phase matrix. The electrochemical techniques showed that the corrosion current density (*i*_{corr}) decreases with increasing both SnO₂ nanoparticles percentages and the time elapsed from the preparation of superconductor samples. Cyclic voltammetry (CV) measurements showed that 0.025% SnO₂ containing superconductor is a good choice for electrochemical capacitor applications. The corrosion process was found to be controlled not only by charge transfer, but also by the diffusion process.

Keywords: corrosion behaviour, superconductors, nanoparticles, cyclic voltammetry, humid media, electrochemical impedance.

1. INTRODUCTION

Bi-based superconductor ceramics are considered as important alternatives for many technological and industrial applications [1]. However, the main restrictions of the (SnO₂)_x(Bi_{1.6}

$\text{Pb}_{0.4}\text{Sr}_2\text{Ca}_2\text{Cu}_3\text{O}_{10-8}$, $(\text{SnO}_2)_x$ (Bi,Pb)-2223, superconductor phase application are the inter grain weak links, weak flux pinning capability, as well as weathering and degradation [2-4]. Corrosion resistance and weathering of superconductors play a significant role in determining the suitability of these materials for various potential applications, and the extent of the need for protective measures in each case. This corrosion resistance of superconductors is important in illustrating the limitations that could be encountered by the use of such materials in various environments, especially in humid media. Such media weakens the mechanical properties of superconductors and increases their weight due to water adsorption and formation of different corrosion products [4]. As a result, the corrosion investigation of superconductors appears to be very significant since these oxide materials are meta-stable and rather reactive as a result of the existence of transition metal ions in high valence states [5]. Several attempts were done in order to enhance phase purity, grain alignment, and magnetic, superconducting, and electrical properties [2, 3]. The addition of nano-oxides such as Al_2O_3 , Zr_2O_3 , NiO , Fe_2O_3 , and SnO_2 to the superconductors proved to be one of the most efficient methods in enhancing their superconducting and mechanical properties [2, 6, 7]. Thus, it is necessary to determine the suitability of (Bi, Pb)-2223 phase superconductors for various technologies and industrial applications and to evaluate the influence of the added nanoparticles to (Bi, Pb)-2223 phase on the corrosion resistance of the superconducting phase.

In our previous work [8] the corrosion behaviour of these superconductors in simulating seawater solutions was examined. However, the present work provides a full characterization of the prepared samples and aims to explore the impact of the incorporation of SnO_2 nanoparticles to $(\text{SnO}_2)_x$ (Bi, Pb)-2223 superconductor in $0.1 \text{ mol L}^{-1} \text{ Na}_2\text{SO}_4$ solutions at $30 \text{ }^\circ\text{C}$ simulating 100 % humid atmosphere.

2. EXPERIMENTAL TECHNIQUES

2.1. Working electrode preparation

The conventional solid-state reaction technique was used to prepare the superconducting samples of the type $(\text{SnO}_2)_x(\text{Bi}_{1.6} \text{Pb}_{0.4})\text{Sr}_2\text{Ca}_2\text{Cu}_3\text{O}_{10-8}$ that is abbreviated as $(\text{SnO}_2)_x(\text{Bi, Pb})$ -2223, where $x = 0.00, 0.025, \text{ and } 0.1 \text{ wt.}\%$. Detailed preparation technique was mentioned in previous work [9].

2.2. Solution Preparation

Distilled water and sodium sulphate (Na_2SO_4) purchased from Sigma-Aldrich chemical industries were used to prepare the test solutions.

2.3. Samples characterization

In order to examine the changes in sample morphology of used superconductor electrodes in the absence and presence of different SnO_2 nanoparticles percentages. X-ray diffraction (XRD)

patterns of samples free from and containing different SnO₂ percentages were obtained using the Bruker D8 advance powder diffractometer with Cu-K α radiation ($\lambda = 1.54056 \text{ \AA}$) in the range $10^\circ \leq 2\theta \leq 70$. The scanning electron microscope (SEM) images were examined before immersion in Na₂SO₄ solutions. The SEM images of the samples were taken using JEOL scanning electron microscope JSM-5300, operated at 30 kV, with a resolution power of 4 nm and a magnification range of 5000. The elemental analysis of the prepared samples were determined using an Oxford X-ray micro-probe analysis connected to JEOL JSM-5300 scanning electron microscope.

2.4. Electrochemical studies

Electrochemical impedance (EIS), polarization measurements, and cyclic voltammetry (CV) were achieved using ACM 1709 potentiostat supplied from ACM instruments company (UK). The used cell setup and conditions were similar to that described in previous work, in which a saturated calomel electrode (SCE) was used as the reference electrode and a platinum electrode as the auxiliary electrode [10]. The working electrode consists of the resultant superconductor discs free from and containing different SnO₂ percentages of area 2.01cm². Before polarization, EIS and CV measurements, the working electrode was polished, cleaned and left for 40 min to obtain the equilibrium potential in 0.1 mol L⁻¹ Na₂SO₄ solution. After measurement, the same electrodes were also cleaned, dried and kept in a desiccator for another sequential immersion.

Polarization curve measurements were done within a potential range from (-300 mV) to anodic direction (500 mV). The frequency range for electrochemical impedance spectroscopy (EIS) measurements was 0.01 to 9.6x10⁴ Hz with applied potential signal amplitude of ± 10 mV around the rest potential. CVs were measured from -300 to +500 mV vs. SCE in the 0.1 mol L⁻¹ Na₂SO₄ electrolyte. They were done at different scan rates of 30 mV min⁻¹, 100 mV min⁻¹, as well as 150 mV min⁻¹.

3. RESULTS AND DISCUSSION

3.1. Samples Characterization

The XRD patterns for (SnO₂)_x(Bi, Pb)-2223 samples with x= 0.00, 0.025, and 0.1wt. % are shown in Figure 1. The diffraction patterns indicate that all the samples are well indexed with the tetragonal indices of (Bi, Pb)-2223 dominant phase [9]. The XRD patterns display different peaks that belong to the main phase of (Bi, Pb)-2223, expect 2 peaks corresponding to (Bi,Pb)-2212 and Ca₂PbO₄ phases, respectively. It is well noticed that there are no peaks detected from impurity phases containing SnO₂ or Sn-rich compounds in XRD patterns. This indicates that SnO₂ nanoparticles did not enter the crystalline structure of (Bi, Pb)-2223, but just occupies interstitial positions between the superconducting grains [9]. Such behavior is confirmed by the values of the lattice parameters (a and c) of the samples given in Table 1. Nearly, the same lattice parameters were obtained for the both pure and SnO₂ nanoparticles-added samples.

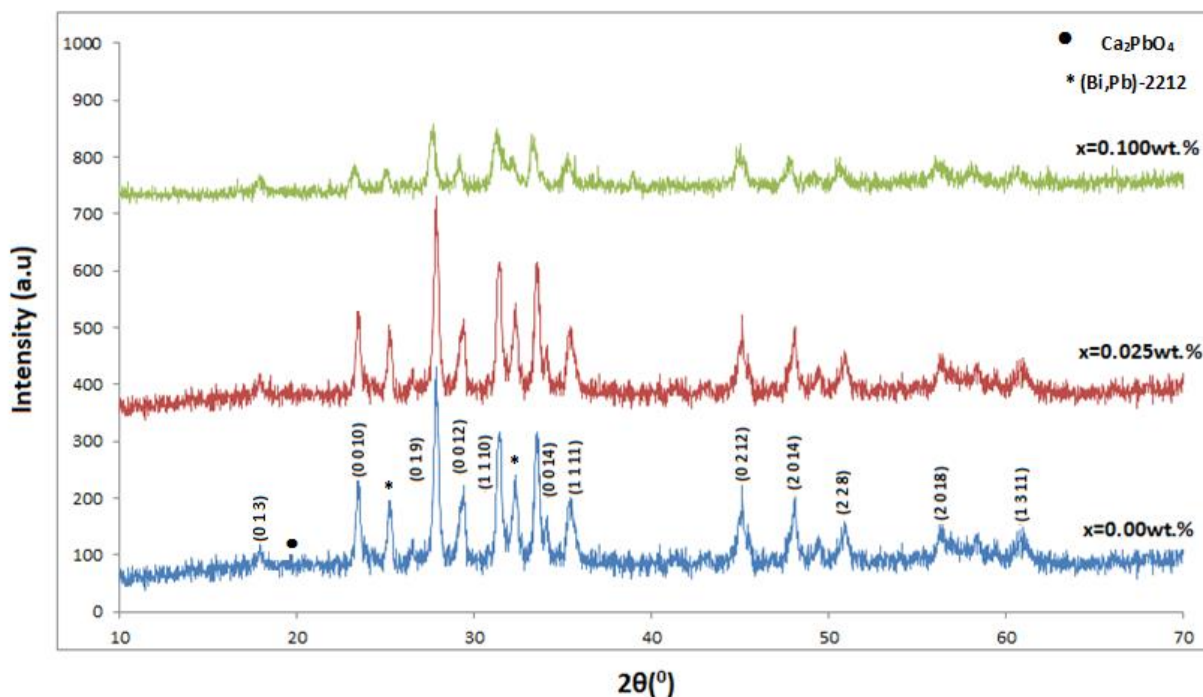


Figure 1. X-ray diffraction patterns for (Bi,Pb)-2223 phase superconductors in the absence and presence of different SnO₂ nanoparticles percentages

Table 1. Lattice parameters for (Bi,Pb)-2223 samples free from and containing different percentages of SnO₂ nanoparticles

SnO ₂ percentage (%)	Lattice Parameters (Å ^o)	
	a	c
0	5.400	36.933
0.025	5.4135	36.956
0.1	5.437	36.951

Figure 2 shows typical SEM images of (SnO₂)_x(Bi, Pb)-2223 phase superconductors with (a) x= 0.00 wt.%. (b) x = 0.025 wt.%. (c) x = 0.10 wt.%. Figure 2a shows, for pure (Bi, Pb)-2223, a well-connected plate-like grains randomly oriented in all directions [9]. Figures (2b and 2c) explains that the addition of SnO₂ does not change the morphological shape of superconductor’s grains. The appearance of white patches in 2b are probably due to the sticking of SnO₂ nanoparticles on the grain or grain boundaries. Figure 2(b) shows that the inter-grain voids decreases upon adding 0.025 wt%. SnO₂. However, the addition of 0.1 wt.%. SnO₂ nanoparticles (Figure 2(c)) causes aggregation and agglomeration of SnO₂ nanoparticles [9]. Figure 3 shows the transmission electron microscope (TEM) image of (SnO₂)_x(Bi, Pb)-2223 phase superconductors with x=0.10 wt.%. Black patches represent the plate-like grains of (Bi,Pb)-2223 phase superconductor grains, whereas small gray particles randomly distributed at grain boundaries represent SnO₂ nanoparticles of

diameter 8.21nm. This result indicates that the added SnO₂ particles are within the nanosized scale, which are located on interstitial positions between the superconducting grains.

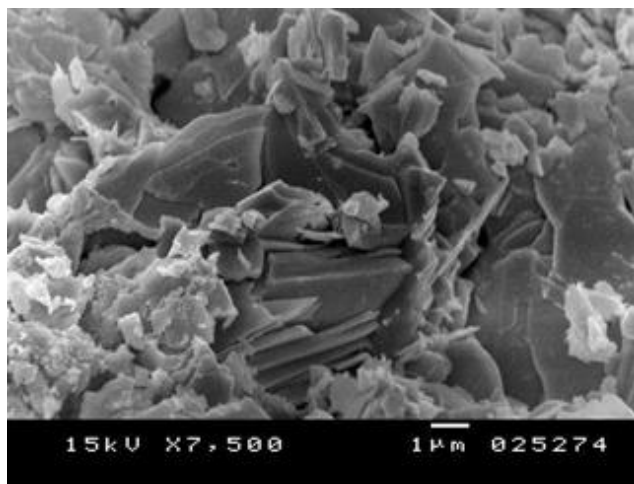


Figure 2(a)

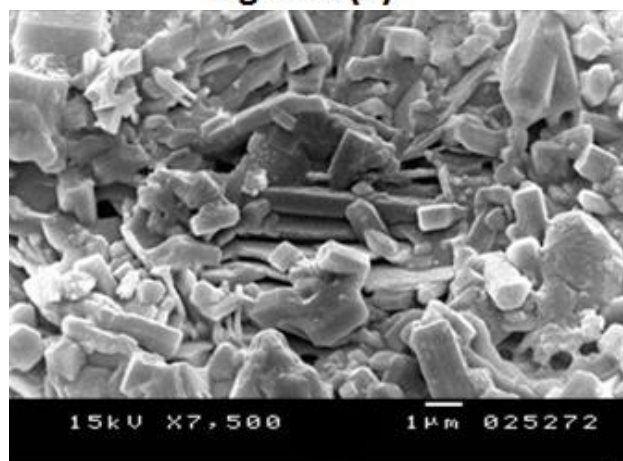


Figure 2(b)

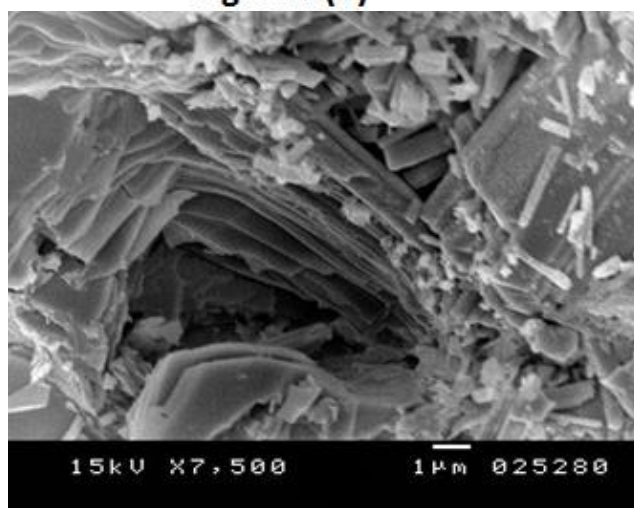


Figure 2(c)

Figure 2. SEM images of (SnO₂)_x(Bi, Pb)-2223 phase superconductors (a) x=0.00 wt %. (b) x=0.025 wt %. (c) x=0.10 wt %.

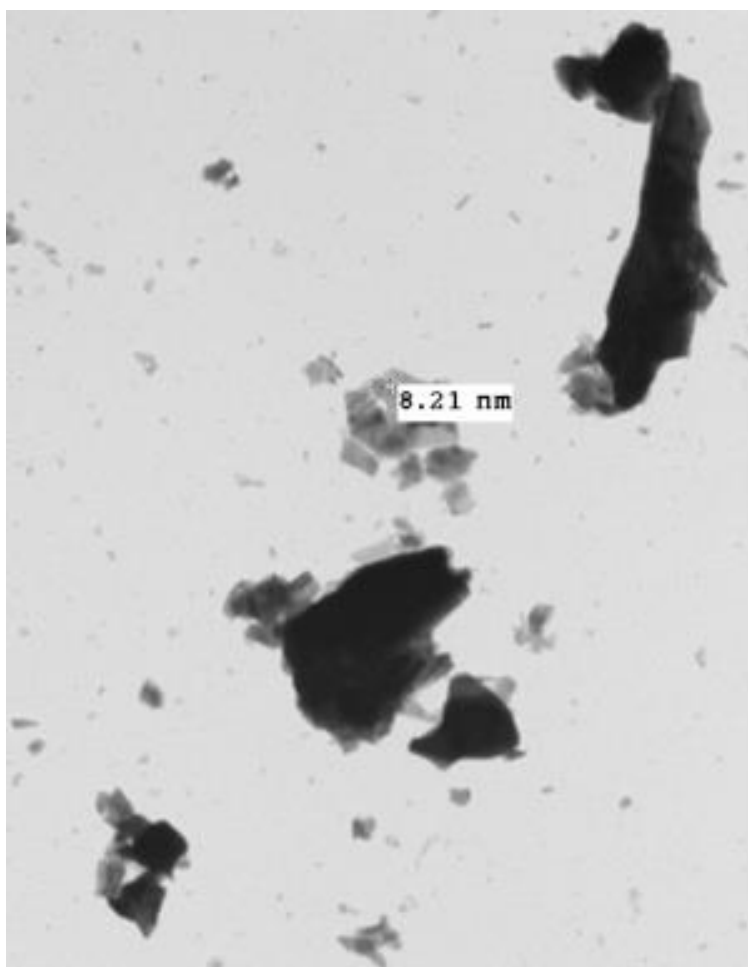


Figure 3. TEM image for (Bi,Pb)-2223 containing 0.1 wt % . nanosized SnO₂ nanoparticles

3.2. Potentiodynamic polarization curves measurements.

Figure 4 shows the potentiodynamic polarization curves of (Bi, Pb)-2223 phase superconductor containing different percentages of SnO₂ nanoparticles in 0.1 mol L⁻¹ Na₂SO₄ at 30 °C. The curves show that the incorporation of SnO₂ nanoparticles shifts the corrosion potential (E_{corr}) to more negative values and suppresses both anodic and cathodic parts of the polarization curves. This indicates that the addition of SnO₂ nanoparticles acts as a mixed type inhibitor for the corrosion of (SnO₂)_x(Bi, Pb)-2223 superconductors in a humid atmosphere.

To ensure the stability of the prepared samples with the time elapsed from their preparation, the polarization curve measurements were repeated for the electrodes containing 0, 0.025 and 0.1 wt. % SnO₂ at different time intervals. Figure 5 shows that time affects predominantly the anodic parts of the potentiodynamic polarization curves for (Bi, Pb)-2223 phase superconductor doped with 0.025 wt. % SnO₂ nanoparticles in 0.1 mol L⁻¹ Na₂SO₄ at 30 °C. A similar observation was recorded for 0 and 0.1 wt. % SnO₂ containing superconductors (not shown).

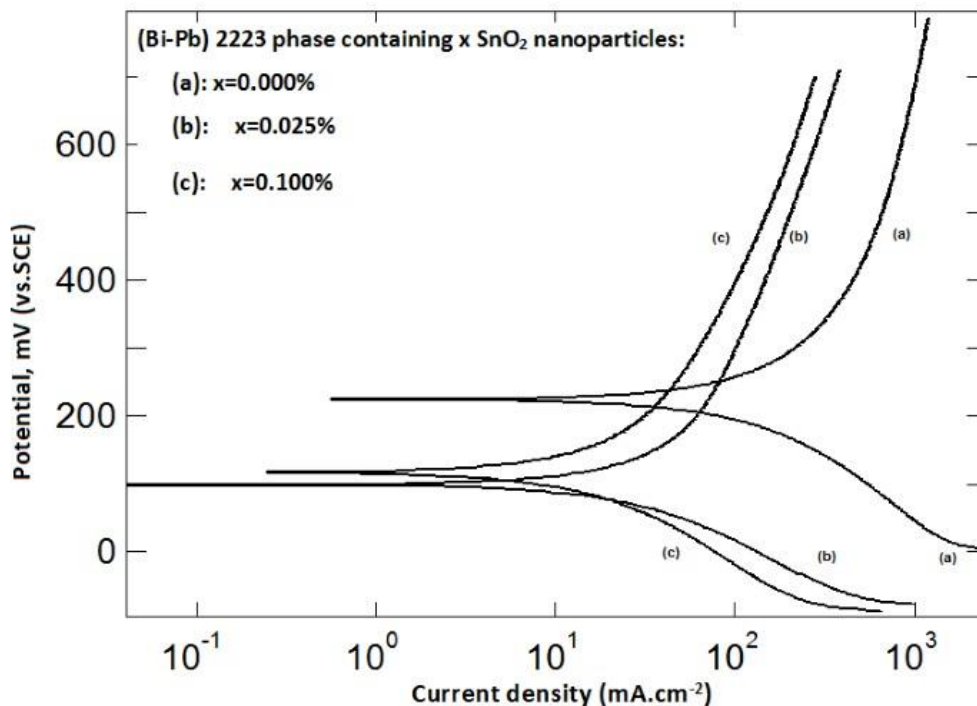


Figure 4. Potentiodynamic polarization curves of (Bi,Pb)-2223 phase Superconductor containing different percentages of SnO₂ nanoparticles in 0.1 mol L⁻¹ Na₂SO₄ at 30 °C.

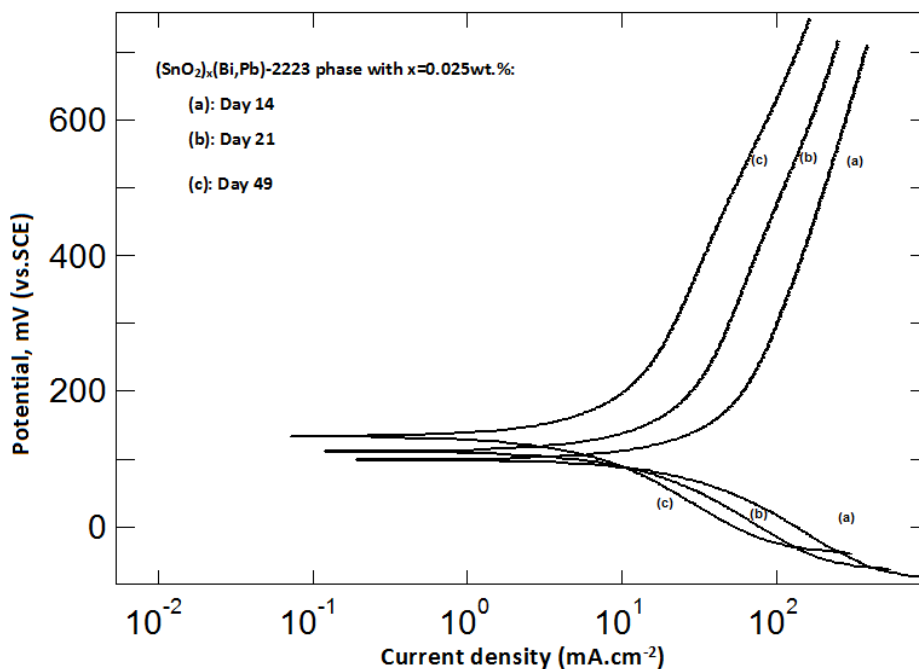


Figure 5. Potentiodynamic polarization curves of (Bi, Pb)-2223 phase Superconductor containing 0.025%.wt. SnO₂ nanoparticles in 0.1 mol L⁻¹ Na₂SO₄ at 30 °C at different time intervals.

The variation of the corrosion current density (i_{corr}) obtained from the analysis of Tafel lines of polarization curves as a function of time is shown in Figure 6. Generally, it is noted that (Bi,Pb)-2223

phase superconductor free from SnO₂ nanoparticles displays a highly corrosive behavior which is attributed to the existence of pores that act as active sites for the initiation of corrosion process [11]. The existence of pores in pure (Bi,Pb)-2223 superconducting samples is evidenced by SEM images. A sharp drop of i_{corr} was observed as time increases to reach 20 days, afterwards, the stability of i_{corr} was noticed. Such decrease is attributed to the formation of corrosion products over the electrode surface hindering the contact of the surface with the electrolyte, and thus reducing the corrosion rate. A similar observation was reported by Qiao *et al* [12] during his investigation of the corrosion behavior B₄C composite ceramics in simulated seawater. Moreover, the enhancement in the anti-corrosion properties of superconductors containing SnO₂ nanoparticles can be referred to the dielectric behavior of these nanoparticles [12].

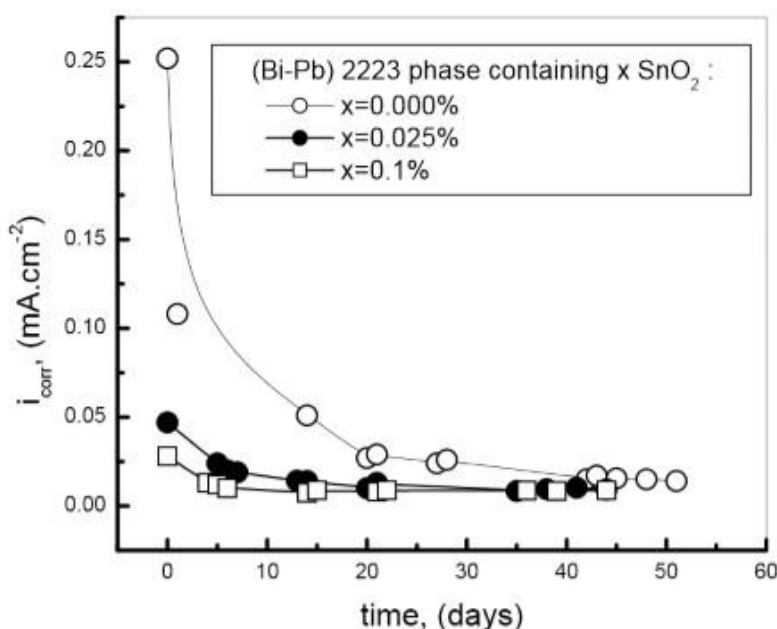


Figure 6. Variation of the corrosion current density as function of time of samples preparation of (Bi,Pb)-2223 phase Superconductors containing different percentages of SnO₂ nanoparticles in 0.1 mol L⁻¹ Na₂SO₄ at 30 °C.

3.3. Cyclic voltammetry measurements (CV)

Figure 7 shows CVs of (Bi, Pb) - 2223 phase superconductor containing different percentages of SnO₂ nanoparticles in 0.1 mol L⁻¹ Na₂SO₄ at 30 °C at a scan rate of 30 mV min⁻¹.

The obtained CV's looks like a quasi-rectangular profile that exhibit mirror symmetry in shape, suggesting an ideal capacitive behavior of (SnO₂)_x(Bi, Pb)-2223 superconductor [13,14]. Such quasi-rectangular shape indicates that the mechanism of charge stored in the (Bi, Pb)-2223 phase is due to the contribution of both electric double layer capacitance and Faradaic reactions (pseudocapacitance) on the overall capacitance [15,16].

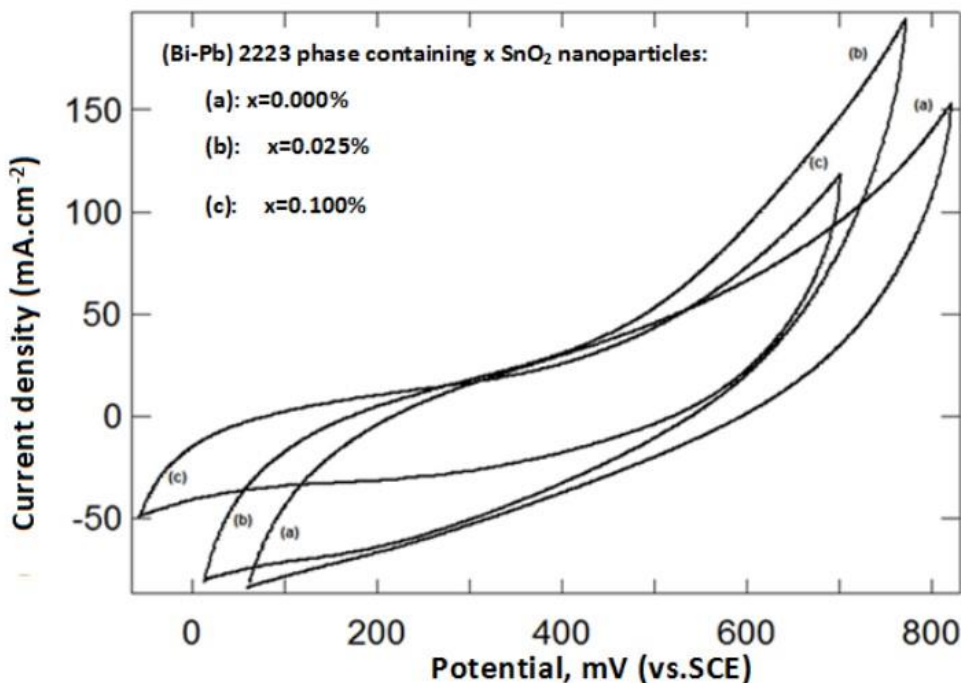


Figure 7. cyclic voltammograms of (Bi,Pb)- 2223 phase Superconductor in the absence and presence of different percentages of SnO₂ nanoparticles in 0.1 mol L⁻¹ Na₂SO₄ at a scan rate of 30 mV min⁻¹ at 30 °C.

Table 2. variation of the specific capacitance (mA cm⁻² mV⁻¹) of (SnO₂)_x(Bi,Pb)-2223 phase Superconductor containing 0.0, 0.025, and 0.1 %. wt. of SnO₂ nanoparticles as function of different scan rates (mV min⁻¹) of at 30 °C.

SnO ₂ wt. %	Scan rate(mV min ⁻¹)	Specific Capacitance (mA cm ⁻² mV ⁻¹)
0.00	30	45
	100	39
	150	51
0.025	30	46
	100	47
	150	56
0.100	30	30
	100	42
	150	44

Table 2 shows the variation of the specific capacitance (mA cm⁻² mV⁻¹) of (SnO₂)_x(Bi, Pb)-2223 phase superconductor with x = 0.00 wt. %, 0.025 wt. %, and 0.10 wt. % as a function of different scan rates (mV min⁻¹) at 30 °C. It is well known that the specific capacitance of an electrode is directly proportional to the area of its CV [17]. Therefore, it is expected that increasing SnO₂ nanoparticles content, increases the specific capacitance of (Bi, Pb)-2223 electrodes. It was found that the addition of 0.025 wt. % SnO₂ can improve the capacitive performance of (Bi, Pb)-2223

composites. This is believed to originate from a higher conductivity of SnO₂ nanoparticles, which is related to the improved electronic conductivity of the electrode materials and the nanostructured morphology of the added SnO₂ particles [18].

However, the addition of 0.1 wt. % of SnO₂ nanoparticles resulted in a decrease in the specific capacitance which might be due to the excess amount of nanoparticles, which further leads to severe aggregation in the superconductor phase. Similar results were obtained by Song *et al* [19] in his study of the electrochemical performance of Co₃O₄/reduced graphene oxide nanosheet composites for supercapacitors. Therefore, 0.025 wt. % SnO₂ containing superconductor may be a good choice as an electrode material for electrochemical capacitor applications.

3.4. Electrochemical Impedance spectroscopy

The Nyquist impedance responses of different (Bi, Pb)-2223 electrodes in the presence and absence of different SnO₂ nanoparticles percentages in 0.1 mol L⁻¹ Na₂SO₄ are shown in figure 8. A depressed capacitive semicircle in the high-frequency range followed by a straight line that indicates the presence of Warburg impedance in the low-frequency range. The appearance of a depressed semicircle denotes the interfacial charge-transfer process occurring at the electrode/electrolyte interface, whereas the straight line at low-frequency range signifies the rapid ion diffusion in the electrolyte and adsorption onto the electrode surface, and suggests the ideally pure capacitive behavior of the electrodes [20, 21].

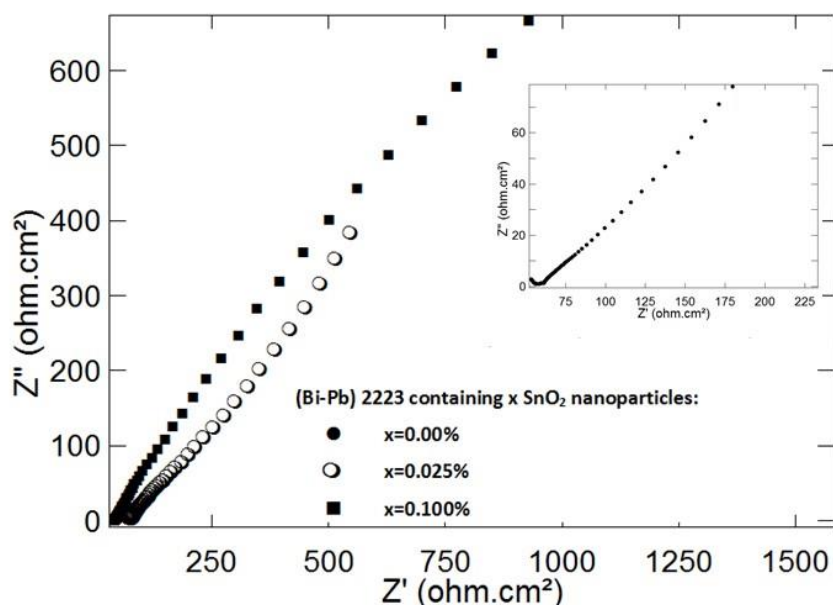


Figure 8. Nyquist impedance plots for (Bi,Pb)-2223 phase Superconductor in the absence and presence of different percentages of SnO₂ nanoparticles in 0.1 mol L⁻¹ Na₂SO₄ at 30 °C.

Figure 9(a-c) shows the equivalent circuit models used to analyze the impedance plots for $(\text{SnO}_2)_x(\text{Bi, Pb})\text{-2223}$ phase superconductors with (a) $x = 0.00$ wt. %. (b) $x = 0.025$ wt. %. (c) $x = 0.10$ wt. % respectively. Generally, these circuits fall into parallel and series capacitor, resistor, and Warburg impedance combinations. The elements of these used circuits are well described by Abdel-Gaber *et al* in previous works [22,23]. R_s denotes solution resistance, R_{ct} charge transfer resistance which is a measure of electron transfer across the surface and inversely proportional to corrosion rate, CPE is the constant phase element and W is the Warburg diffusion impedance.

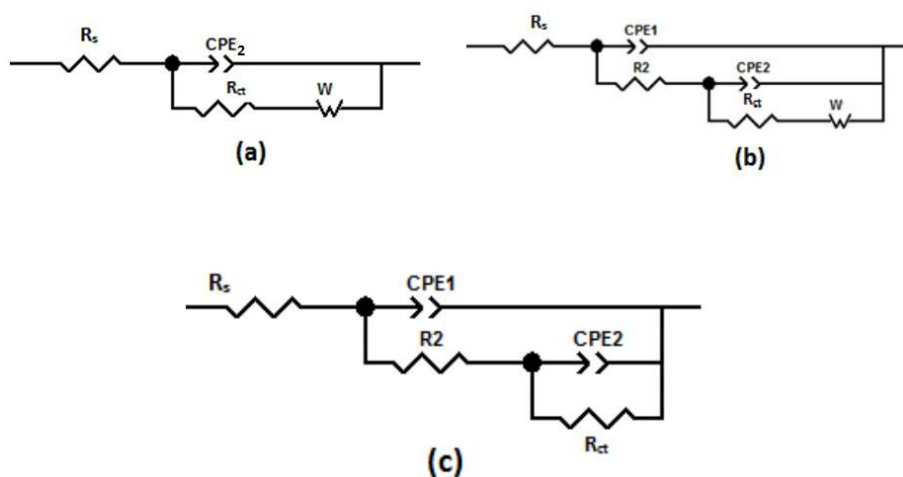


Figure 9. Schematic for the equivalent circuit models for $(\text{SnO}_2)_x(\text{Bi,Pb})\text{-2223}$ phase superconductors (a) $x = 0.00$ wt. %. (b) $x = 0.025$ wt. %. (c) $x = 0.10$ wt. %.

The fitting of the spectrum to the equivalent circuit models permits the evolution of the elements of the circuit analogue. The experimental and computing fit results of the Nyquist plot of 0.025 wt. % SnO_2 containing superconductor in $0.1 \text{ mol.L}^{-1} \text{ Na}_2\text{SO}_4$ at $30 \text{ }^\circ\text{C}$ is demonstrated in Figure 10.

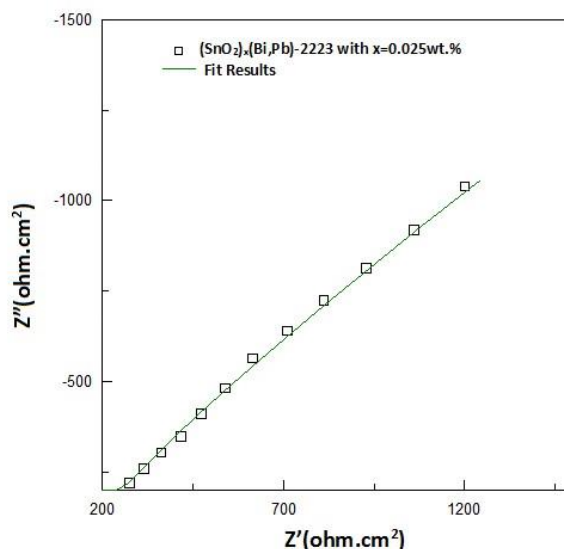


Figure 10. The experimental and computer fit results of Nyquist plot of $(\text{Bi,Pb})\text{-2223}$ phase superconductor containing 0.025 wt. % SnO_2 in $0.1 \text{ mol L}^{-1} \text{ Na}_2\text{SO}_4$ at $30 \text{ }^\circ\text{C}$.

The values of the electrochemical impedance parameters obtained from the fitting of the experimental data for the corrosion (Bi, Pb)-2223 phase superconductors containing different percentages of SnO₂ nanoparticles in 0.1 mol L⁻¹ Na₂SO₄ at 30 °C to the used equivalent models are presented in Table 3. As seen from Table 3, the charge transfer resistance (R_{ct}) increases as the SnO₂ nanoparticles percentages in (Bi, Pb)-2223 phase superconductor increases. This indicates that (Bi, Pb)-2223 phase superconductor containing SnO₂ nanoparticles exhibit more corrosion resistance than (Bi, Pb)-2223 superconductors free from SnO₂ nanoparticles [24].

Table 3. Electrochemical impedance parameters for the corrosion of (Bi,Pb)-2223 phase Superconductor in the absence and presence of different percentages of SnO₂ nanoparticles in 0.1 mol L⁻¹ Na₂SO₄ at 30 °C.

SnO ₂ wt.%	Time (Days)	R_s (ohm cm ²)	Q_1 (F cm ⁻²)	n_1	R_2 (ohm cm ²)	Q_2 (F cm ⁻²)	n_2	R_{ct} (ohm cm ²)	W_R	W_T	W_P
0	21	120	-	-	-	18×10^{-4}	0.64	156	1832	140	0.41
	49	168	-	-	-	5.5×10^{-4}	0.82	169	4737	108	0.47
0.025	21	92	0.0023	0.54	55	7.2×10^{-5}	0.87	2554	999	5.8	0.29
	49	110	0.0013	0.59	2412	3.8×10^{-5}	0.95	3211	4500	31.0	0.50
0.100	21	58	0.0017	0.62	1720	0.0017	0.54	4940	-	-	-
	49	87	0.0011	0.62	2310	0.0018	0.56	7340	-	-	-

Moreover, it is clearly observed that the time influences predominantly the corrosion behavior of (Bi, Pb)-2223 phase superconductors. It is noted that the charge transfer resistance R_{ct} for (SnO₂)_x(Bi,Pb)- 2223 phase superconductor with $x = 0.00$ wt.%, $x = 0.025$ wt. %, and $x = 0.10$ wt.% increases throughout the whole test period, indicating that its corrosion resistance is enhanced as the time elapsed from the sample preparation increase. This may be due to the reducing of the uncovered area available for charge transfer due to corrosion product formation on the phase surface. These results showed that the formation of scale products on the electrode surface is strengthened with time [25]. Such phenomena are confirmed by the decrease in the non-ideal double layer capacitances (Q_1 and Q_2) that signifies a valid evidence for the formation of corrosion products film that covers the phase surface, and that these products grow as time proceeds. This behavior has been associated with the plate capacitor model, where the surface capacity film (C) is inversely proportional to its thickness d , [$C = \epsilon_0 \epsilon / d$], where ϵ_0 is the permittivity of a vacuum; and ϵ is the relative permittivity of the film) [26]. Hence, the reduction of Q_1 and Q_2 with time matches the corresponding increase in the thickness of the scale products on the phase surface, and the enhancement of the protective properties of this film is formed. The values of n_1 associated with Q_1 are found in the 0.54–0.62 interval revealing that the occurrence of the diffusion process. Whereas different values of n_2 are due to the modification of the structure of the corrosion products film in combination with its thickness, as suggested by the R_{ct} values [27].

Since in the diffusion interpretation $W_T = L^2/D$, where (L is the effective diffusion thickness, and D is the effective diffusion coefficient of the particle) [28]. It is noted that the increasing W_T values in the presence of SnO₂ nanoparticles could possibly be related to increasing the diffusion thickness, and vice versa in the absence of nanoparticles.

The obtained impedance data are in fairly good agreement with the results obtained previously from polarization measurements. Both techniques confirm the substantial role of SnO₂ nanoparticles in reducing the corrosion of (Bi, Pb)-2223 superconductors in humid environments.

3.5. Corrosion and Inhibition Mechanism

Galvanic corrosion is the most common type of corrosion among (SnO₂)_x(Bi,Pb)-2223 phase superconductor matrices due to their metallic variety. Such form of corrosion in (SnO₂)_x(Bi,Pb)-2223 phase superconductor relies on the potential of its metallic composition. By comparing the potential of the chemical ingredients of the superconductor material [29], it was noted that Strontium (Sr), calcium (Ca) and lead (Pb) are easily dissolved at the anodic site. However, copper (Cu), Bismuth (Bi), and Tin oxide (SnO₂), are reduced at the cathodic site. The incorporated SnO₂ nanoparticles are easily reduced to Sn. The resultant Sn decreases the voids, pores present in the phase matrix and modifies the phase surface, thus shifting the corrosion rate to lower values and inhibiting the corrosion of (Bi-Pb)-2223 phase superconductor.

4. CONCLUSION

The addition of SnO₂ nanoparticles enhances the electrochemical and capacitive behavior of (Bi,Pb)-2223 phase superconductor and preserve their durability in humid environments. Such nanosized particles serve as an efficient corrosion inhibitor for (Bi, Pb)-2223 phase superconductor in humid media, thus extending superconductor's lifespan and promoting technological developments in many fields. Moreover, the incorporation of 0.025 wt. % SnO₂ is a good choice for electrochemical capacitor applications.

ACKNOWLEDGEMENTS

The authors thank the Superconductivity and Metallic Glasses Lab in Alexandria University as well as Dr. Mai Barakat for their assistance in sample characterization.

References

1. B. Özçelik, M. Gürsul, A.Sotelo and M.A. Madre, *J. Mater. Sci. Mater. Electron.*, 26 (2015) 441.
2. R.Awad, A.I. Abou-Aly, M.A.Gawad and I. G-Eldeen, *J. Supercond. Nov. Magn.*, 25 (2012) 739.
3. J.Taghipour, H.Abbasi and H.Sedghi, *Physica B: Condens. Matter.*, 405 (2010) 1349.
4. D.E. Clark and B.K. Zoitos, *Corrosion of glass, ceramics and ceramic superconductors: principles, testing, characterization and applications*. Park Ridge, Noyes Publications (1992) New Jersey, USA.
5. R.Börner, W.Paulus, R. Schöllhorn, B. Kabius and J.Schubert, *Adv. Mater.*, 7 (1995) 55.
6. A. Mellekh , M. Zouaoui , F.B.Azzouz, M. Annabi and M.B.Salem, *Solid State Commun.*,140 (2006) 318.
7. B.A. Albiss, I.M. Obaidat, M.Gharaibe, H. Ghamlouche and S.M. Obeidat, *Solid State Commun.*, 150 (2010) 1542.

8. H.T. Rahal, A.M. Abdel-Gaber and R. Awad, *Chem. Eng. Commun.*, 204 (2017) 348.
9. H.T.Rahal, R. Awad, A.M.Abdel-Gaber and M. Roumie, *J. Supercond. Nov. Magn.*, 30 (2017)1971.
10. H.T.Rahal, A.M.Abdel-Gaber and G.O. Younes, *Chem. Eng. Commun.*, 203 (2016) 435.
11. A.B.Radwan, R.A.Shakoor and A. Popelka , *Int. J. Electrochem. Sci.*, 10 (2015)7548.
12. Y.Qiao, L.Qu, X.Zhang and H.Zhang, *Ceram. Int.*, 41 (2015) 5026.
13. J. Zhu and H. Junhui H, *ACS. Appl. Mater. Interfaces*, 4 (2012) 1770.
14. X.Zhao, Y.Du, Y.Li and Q., *Ceram. Int.*, 41 (2015) 7402.
15. C.Pan, G.Haiteng, and D. Li, *J. Power Sources*, 303 (2016)175.
16. K. Krishnamoorthy, S.Thangavel, J.C.Veetil, N.Raju, G.Venugopal and S.J. Kim , *Int. J. Hydrogen Energy*, 41(2016)1672.
17. Y.Xiong,M. Zhou,H.Chen,L.Feng, Z.Wang, X.Yan and S.Guan , *Appl. Surf. Sci.*, 357 (205) 1024.
18. L.Ma, X.Shen, Z. Ji, G.Zhu and H. Zhou, *Chem.Eng. Commun.*, 252 (2014) 95.
19. Z.Song, Y.Zhang, W. Liu,S. Zhang, G.Liu, H.Chen and J. Qiu, *Electrochim. Acta*, 112 (2013) 120.
20. A. Ramadoss and J.K., *Carbon*, 63(2013) 434.
21. H.Tian,Y.F. Cheng, W.Li and B. Hou , *Corros. Sci.*, 100 (2015) 341.
22. A.M.Abdel-Gaber, B.A. Abdel-Nabey and M. Saadawy , *Mater. Corros.*, 63 (2012)161-167.
23. A.M.Abdel-Gaber,B.A. Abd-El-Nabey, E.Khamis and D.E.Abd-El-Khalek, *Desal.*, 230 (2008) 314.
24. R. Govindasamy and S.Ayappan, *J. Chil .Chem. Soc*, 60 (2015) 2786.
25. R. Tourir, N.Dkhireche, M.E.Touhami, M.Lakhrissi, B.Lakhrissi and M. Sfaira, *Desal.*, 249 (2009) 922.
26. N. El-Bagoury, M.A. Aminand H. Shokry, *Int. J. Electrochem. Sci.*, 8 (2013) 1246-1261.
27. L. Vrsalović, S. Gudić, and M. Kliškić, *Indian J. Chem. Technol.*, 19 (2012) 96-102
28. ZView2 help, Scribner Associates. 2000
29. D.R. Lide, CRC handbook of chemistry and physics (2004) CRC press.

© 2017 The Authors. Published by ESG (www.electrochemsci.org). This article is an open access article distributed under the terms and conditions of the Creative Commons Attribution license (<http://creativecommons.org/licenses/by/4.0/>).